JVST A
Journal of Vacuum Science & Technology A

Multilayer ultraviolet reflective coating based on atomic layer deposited aluminum oxide and fluoride

Cite as: J. Vac. Sci. Technol. A **39**, 042402 (2021); https://doi.org/10.1116/6.0001010
Submitted: 04 March 2021 • Accepted: 06 May 2021 • Published Online: 04 June 2021

Zhiyu Huang, Daniel C. Messina, Brianna S. Eller, et al.

COLLECTIONS

Paper published as part of the special topic on Atomic Layer Deposition (ALD)

F This paper was selected as Featured

SCI This paper was selected as Scilight

View Online

Export Citation

CrossMark

ARTICLES YOU MAY BE INTERESTED IN

Thermal atomic layer etching of amorphous and crystalline Al_2O_3 films
Journal of Vacuum Science & Technology A **39**, 042602 (2021); https://doi.org/10.1116/6.0000995

UV-coated optical filters for space based optical systems to study space-based processes
Scilight **2021**, 231107 (2021); https://doi.org/10.1063/10.0005307

Review Article: Stress in thin films and coatings: Current status, challenges, and prospects
Journal of Vacuum Science & Technology A **36**, 020801 (2018); https://doi.org/10.1116/1.5011790

© 2021 Author(s).

ARTICLE

avs.scitation.org/journal/jva

Multilayer ultraviolet reflective coating based on atomic layer deposited aluminum oxide and fluoride

Cite as: J. Vac. Sci. Technol. A **39**, 042402 (2021); doi: 10.1116/6.0001010
Submitted: 4 March 2021 · Accepted: 6 May 2021 ·
Published Online: 4 June 2021

View Online

Export Citation

CrossMark

Zhiyu Huang,[1] Daniel C. Messina,[1] Brianna S. Eller,[1] Franz A. Koeck,[1] Paul A. Scowen,[2] and Robert J. Nemanich[1,a)]

AFFILIATIONS

[1]Department of Physics, Arizona State University, Tempe, Arizona 85287-1504
[2]School of Earth and Space Exploration, Arizona State University, Tempe, Arizona 85287-6004

Note: This paper is part of the 2022 Special Topic Collection on Atomic Layer Deposition (ALD).
[a)]**Electronic mail:** robert.nemanich@asu.edu

ABSTRACT

Ultraviolet optical coatings employ wide bandgap dielectric materials due to their characteristic low absorption. High-reflectivity and antireflective coatings are essential for optical devices, which can be achieved by alternately depositing two dielectrics with different refractive indices. In this research, a multilayer high-reflectivity coating has been designed for middle UV wavelengths using Al_2O_3 and AlF_3 layers on a sapphire (0001) substrate, and the initial two-layer structure has been fabricated by atomic layer deposition. The surface morphology and roughness of the coating was measured by atomic force microscopy after each deposition step. Ultraviolet spectroscopy and spectroscopic ellipsometry were used to characterize the optical performance of the single and multilayer coatings. Monochromatic x-ray photoemission spectroscopy was used to study the film composition, bonding, and impurities. A bilayer reflective coating was demonstrated, with a smooth surface ($R_q < 1$ nm) and peak reflectance of 25%–30% at a wavelength of 196 nm. The measured reflectance deviated from the simulations in the middle UV range, and an analysis of the AlF_3 layer prepared by plasma enhanced atomic layer deposition indicated the presence of Al-rich clusters, which were associated with the UV absorption. A thermal atomic layer deposition process for AlF_3 deposition showed reduced absorption, which could be more effective for shorter wavelength designs.

Published under an exclusive license by the AVS. https://doi.org/10.1116/6.0001010

I. INTRODUCTION

Thin-film optical coatings, especially for high-reflectivity (HR) and antireflective (AR) applications, are commonly used in the fields of space science,[1–5] laser physics,[6,7] and photonic devices.[8–10] Optical coatings applied in the ultraviolet (UV) wavelength regime are more challenging than those in the visible or near infrared, as most of the coating materials suffer from significant absorption in the UV range. HR coatings are fundamental for optical filters.[11] Specifically, for UV bandpass filters based on a Fabry–Pérot interferometric design, the metal reflective layers can be replaced by dielectric layers with lower absorption.[5,11] Thus, low-absorption high-reflectivity coatings are key for the design and fabrication of UV-based optical devices. The search for materials meeting these requirements has gained interest in the optics and material physics communities.[11–14]

Dielectrics, especially metal fluorides, have garnered much attention in UV optics, due to their wide bandgaps and low cutoff wavelengths.[2–4,15] One method to achieve AR or HR coatings is to alternately deposit two dielectrics with different refractive indices.[11] In the visible and near infrared regime, metal oxides have been largely used, with the high refractive index layers (H-layers) of Al_2O_3,[7,16,17] Ta_2O_5,[10,18,19] ZrO_2,[18] HfO_2,[6,9,20] or TiO_2,[19] while the low refractive index layers (L-layers) are normally SiO_2.[9,17,18]

However, most metal oxides display poor UV optical performance due to absorption below each oxide's cutoff wavelength, typically below 250 nm. To extend the use of oxides into the UV, metal fluorides have been identified as a key material for next generation UV coatings and optical systems.[3,4,15] For UV optical coatings, BaF_2,[12] LaF_3,[7,12,21] or GdF_3[22] have been used as H-layers, while MgF_2 (Refs. 7, 12, and 21) and AlF_3 (Refs. 16 and 22) have been

Published under an exclusive license by the AVS

used as L-layers. It is also worth noting that the definition of H- and L-layers is not strict, for example, low-index oxides, e.g., SiO_2, have also been used as H-layers when paired with metal fluorides, such as MgF_2.[12] Besides oxides and fluorides, UV optical coatings have also been reported to employ nitrides and carbides including AlN,[23] Si_3N_4,[1] and SiC.[24] A plot of refractive index, n, versus wavelength for frequently used UV optical coating materials is shown in Fig. 1. Values shown in Fig. 1 are obtained from various references.[25–31]

Common deposition techniques for the optical coating industry include physical vapor deposition and chemical vapor deposition (CVD).[32] However, atomic layer deposition (ALD), a subset of CVD, has emerged to be a leading technique for modern semiconductor fabrication, which requires ultrathin high-κ dielectric layers.[33,34] Compared with other thin-film deposition methods, ALD has advantages of precise thickness control, high conformality and uniformity, and subnanometer root-mean-square surface roughness (R_q), which are all at least partially due to the unique self-limiting ALD growth process.[32,33,35–37] Plasma enhanced ALD (PEALD) is an energy-enhanced variation of ALD utilizing plasma radicals to drive surface reactions and reduce the number of surface species prior to initiating each cycle or half-cycle.[38,39]

For UV coating applications, surface roughness becomes increasingly important as surface scattering can significantly degrade the optical performance of the designed coating.[14] Even though ultrasmooth surfaces ($R_q \approx 0.2$ nm) have been achieved using techniques such as sputtering, the incorporation of unwanted impurities may occur.[40] However, the self-limiting growth mechanism for ALD allows for minimal build-up of roughness for amorphous oxide and fluoride films.[41] The smooth surface and precise thickness control benefits thin-film coating design, fabrication, and characterization. As discrete precursor exposures are used in ALD to obtain self-limiting surface reactions, longer deposition times are to be expected in comparison to other growth methods.[32,37]

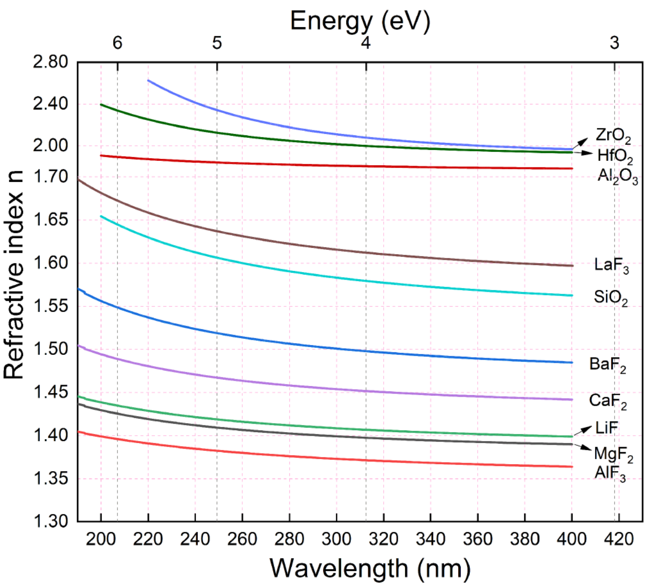

FIG. 1. Refractive index vs wavelength for UV coating materials.

In this study, a reflective coating consisting of single-side polished single-crystal Al_2O_3 (sapphire) substrate and amorphous Al_2O_3 and AlF_3 layers has been modeled and demonstrated for optical applications in the middle UV (200–300 nm) range. The AlF_3 layers were deposited by PEALD and the Al_2O_3 layers by thermal ALD (TALD). PEALD was chosen for AlF_3 as the TALD process, using trimethylaluminum (TMA) and hydrogen fluoride (HF), shows excess HF adsorbed onto the AlF_3 surface after each cycle.[42] As such, a remote H_2 inductively coupled plasma (ICP) was implemented to remove the excess absorbed HF possibly leading to a denser film. The coating was characterized at each step of fabrication using atomic force microscopy (AFM), UV spectroscopy, and spectroscopic ellipsometry (SE). A smooth bilayer reflective coating with UV reflectance of 25%−30%, centered at 196 nm, has been achieved.

However, the properties of the AlF_3 layer were related to a deviation from the predicted optical performance. *In situ* x-ray photoelectron spectroscopy (XPS) and *ex situ* SE were used to characterize a set of PEALD and TALD AlF_3 films to determine the composition, bonding, and defect configurations. Modified simulations could account for the optical performance deviation based on the inclusion of Al-rich clusters in the AlF_3 layer.

II. OPTICAL COATING DESIGN

A multilayer high-reflectivity coating can be constructed based on the traditional Bragg reflector design. In this design, a stack of dielectric layers with alternate high and low refractive indices are used, with each layer fixed at quarter-wavelength optical thickness (QWOT), i.e., $\lambda_{cen}/4n$.[11] Here, λ_{cen} is the central wavelength where the reflectance maxima occur and n is the refractive index at λ_{cen}. The ultimate reflectance R_k of the multilayer coating can be estimated using Eq. (1),[43]

$$R_k = 1 - 2\pi n_0 \frac{k_H + k_L}{n_H^2 - n_L^2}, \qquad (1)$$

where n_0 is the refractive index of incident medium and H and L denote high- and low-index layers, respectively. Equation (1) shows that for transparent materials (where extinction coefficients $k_H = k_L = 0$), the ultimate reflectance can theoretically reach 100%. For the case of $k_H + k_L \neq 0$, the larger the difference of the refractive index, the higher the ultimate reflectance of the coating.

Based on these considerations, the materials for UV reflective coatings should satisfy two conditions: (1) The materials should have relatively large bandgaps, in order to minimize the absorption, and (2) the H-L refractive index contrast should be maximized for ultimate reflectance. In this research, the cutoff wavelength, λ_c, of the materials should be below 300 nm, for middle UV optical applications.

A. High- and low-index materials selection

The refractive index and cutoff wavelength, λ_c, for selecting UV coating materials, are shown in Figs. 1 and 2, respectively. As indicated in Fig. 2, the refractive index increases with λ_c, which

Published under an exclusive license by the AVS

agrees with the energy gap-refractive index correlations described by the Moss relation [Eq. (2a)] and the Herve–Vandamme relation [Eq. (2b)],[44]

$$\text{Moss relation: } n^4 E_g = 95\,\text{eV}, \tag{2a}$$

$$\text{Herve–Vandamme relation: } n^2 = 1 + \left(\frac{13.6\,\text{eV}}{E_g + 3.47\,\text{eV}}\right)^2, \tag{2b}$$

where n and E_g are the refractive index and energy gap, respectively. Values shown in Fig. 2 are obtained from various references.[14,25–31,45–56]

For the selection of H-layer materials, evidently, the commonly used TiO_2, Ta_2O_5, and Nb_2O_5 are no longer feasible due to their lower bandgap energies. In this study, Al_2O_3 was chosen as the H-layer because of its wider bandgap (6.7 eV) and lower UV absorption compared to other high-index materials, such as ZrO_2, HfO_2, and Y_2O_3.[55,56] As for the L-layers, the commonly used SiO_2 in the visible range can be replaced by metal fluorides. Specifically, AlF_3 or MgF_2 have a significantly lower index and larger bandgap (both 10–11 eV)[42,45,57] than SiO_2. These fluorides are projected to be transparent down to 115 nm with refractive indices of ~1.4.[42,57] To minimize the number of layers for the UV coating, AlF_3, Al_2O_3, and (0001) sapphire were chosen as the low-index layer, the high-index layer, and the substrate, respectively.

B. Optical coating modeling

The structure of the reflective coating, which is based on QWOT Al_2O_3 and AlF_3 layers, was designed as vacuum/$(Al_2O_3/AlF_3)^m$/sapphire, where m denotes the number of repeating bilayers [Fig. 3(b)]. For the quarter-wave HR coatings, the top layer must be an H-layer for constructive interference;[11] thus, the lowest order reflective coating is a bilayer structure, i.e., $m = 1$. This coating was designed to be used at wavelengths between 200 and 250 nm with a reflectance maximum and central wavelength at 225 nm. The optical constants used for ALD Al_2O_3 were measured by SE, from a 52 nm thick Al_2O_3 layer prepared by TALD. A transparent Cauchy model,

$$n = \text{A} + \frac{\text{B}}{\lambda^2} + \frac{\text{C}}{\lambda^4}\ (\lambda \text{ in } \mu\text{m}), \tag{3}$$

was used to describe the Al_2O_3 index of refraction. As for the AlF_3 layer, the Cauchy parameters for a 50 nm TALD AlF_3 layer,

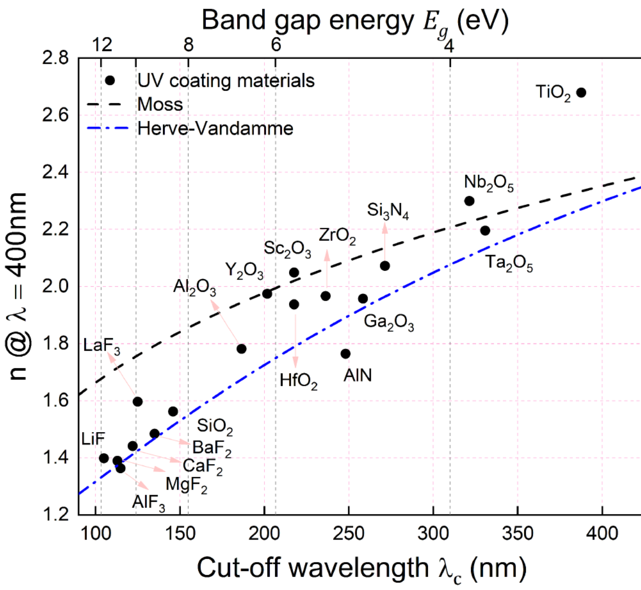

FIG. 2. Refractive index (at λ = 400 nm) vs λ_c and E_g for UV coating materials.

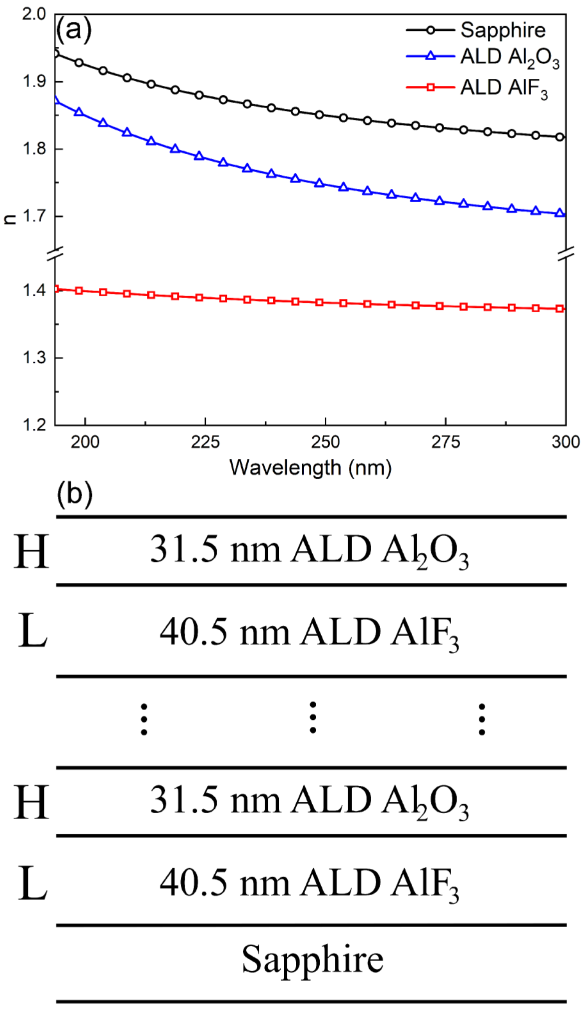

FIG. 3. Design of the Al_2O_3/AlF_3 HR coating. (a) Refractive index of each layer used for the simulation and (b) structure of the coating with thickness of each layer fixed at QWOT. H and L denote H-index and L-index, respectively.

Published under an exclusive license by the AVS

TABLE I. Cauchy parameters used for UV reflective coating design.

Growth method	Material	A	B	C
Thermal ALD	Al_2O_3	1.636	0.0041	1.79×10^{-4}
Thermal ALD	AlF_3	1.352	0.0019	0
	Sapphire	1.757	0.0046	8.36×10^{-5}

reported by Hennessy *et al.*,[31] were used for the modeling. Table I lists the Cauchy parameters used for the sapphire substrate, ALD Al_2O_3, and ALD AlF_3, which are also plotted in Fig. 3(a). The refractive index for sapphire is from Dodge.[27]

The reflectance of the designed coating was simulated using ellipsometry software (J. A. Woollam, COMPLETEEASE v6.51), which is based on the transfer matrix method.[58,59] The simulated reflectance at normal incidence ($\theta = 0°$) (Fig. 4) shows that with increasing number of the repeating bilayers, the ultimate reflectance approaches 100% [in agreement with Eq. (1)], and the ultimate bandwidth ($\Delta\lambda$) approaching the theoretical value of 36 nm is given by Eq. (4),[21]

$$\Delta\lambda = \frac{4}{\pi}\sin^{-1}\left(\frac{n_H - n_L}{n_H + n_L}\right)\lambda_{cen}. \tag{4}$$

In this study, an $m = 1$ reflective coating was fabricated and characterized, and the optical properties were compared to the simulation results. The coating was not extended beyond a single stack due to the long deposition times associated with ALD.

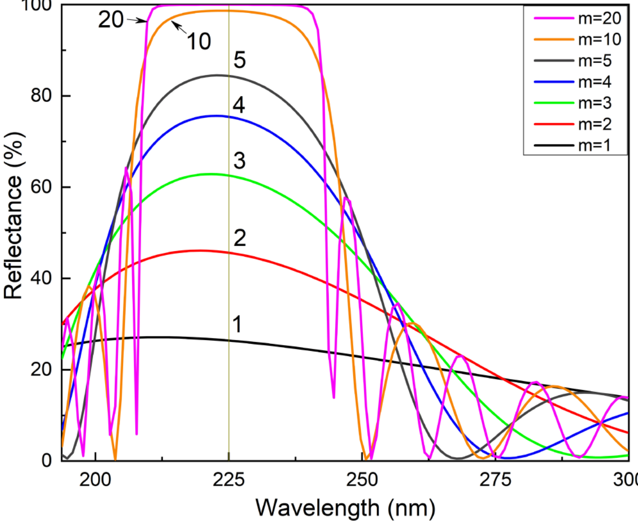

FIG. 4. Simulated reflectance at normal incidence ($\theta = 0°$) with different numbers of the repeating bilayers, with λ_{cen} = 225 nm and $\Delta\lambda$ = 36 nm.

III. EXPERIMENTAL METHODS

The experiments involved ALD AlF_3 layers on passivated Si surfaces and also on sapphire substrates to be used as a UV reflective filter following the design in Fig. 4. During the optical measurements, it was recognized that the PEALD AlF_3 layers exhibited additional UV absorption. Consequently, an alternative thermal ALD process was studied and compared to confirm the effect and explore alternatives. The experimental description presents the experimental details for both the plasma and thermal ALD AlF_3 processes.

AlF_3 films were deposited, by PEALD or TALD, using a custom-built reactor integrated into an ultrahigh vacuum (UHV) cluster tool allowing for *in situ* characterization. The reflective coating was grown on a single-side polished 25.4 mm diameter sapphire wafer (0001) (MSE Supplies, WA0427). Initial PEALD and TALD layers were on 25.4 mm diameter boron-doped silicon wafers (100) (Virginia Semiconductor) passivated with a 33 nm coating of TALD amorphous Al_2O_3. The TALD Al_2O_3 layers were prepared using a commercial tool (Cambridge, Savannah S100) with TMA and H_2O, as precursors, and a substrate temperature of 185 °C. Sample surfaces were cleaned using a 10-min UV-ozone exposure and then placed into the load-locked UHV cluster tool prior to initial characterization.

The plasma and thermal ALD AlF_3 layers were deposited in the same chamber, which is part of the UHV cluster tool described in a previous report.[60] For PEALD, the system is equipped with a 13.56 MHz radio frequency ICP for generating hydrogen radicals. The ALD AlF_3 reactions were performed using TMA (STREM, 97%), hydrogen fluoride-pyridine (HF-P) (Alfa-Aesar, 70 wt. % HF), and H_2 (Matheson Tri-Gas, 5 N) as Al, F, and H precursors, respectively. The ALD process used a substrate temperature of 100 °C. HF-P was chosen based on the results of a prior AlF_3 ALD study where HF-P was shown to be a convenient, less-volatile alternative to handle anhydrous HF.[56,61] Each ALD half-cycle consisted of a precursor exposure and Ar purge. For the PEALD AlF_3 process, an H_2-plasma step was included after each HF step.

Film surface composition, chemical bonding states, and defect configurations were determined by *in situ* XPS. The XPS instrument (VG Scientia, R3000) uses a monochromatic Al K_α x-ray source with a photon energy of 1482 eV. Data acquisition was performed using the manufacturer supplied software (VG Scientia, SES SOFTWARE). The system pressure was below 7×10^{-10} Torr during measurements. High resolution scans of the Al 2p core level were acquired using a pass energy of 200 eV, step size of 0.050 eV, and energy resolution of 0.30 eV. Peak analysis was performed using an XPS software package (Casa Software LTD, CASAXPS). All photoelectron transitions were modeled with Gaussian–Lorentzian line shapes with Tougaard backgrounds.[62] Relative atomic concentrations were calculated using a standard method based on the ratio of peak areas and atomic sensitivity factors and has an accuracy of 10%–20%.[63]

A custom-built vacuum UV spectrometer, with a base pressure 4×10^{-7} Torr, was used for *in situ* characterization of the optical properties spanning 120–300 nm. The UV spectrometer, described previously,[60] has three primary components: a UV light source, a monochromator, and a detector. The light source used is a

Published under an exclusive license by the AVS

water-cooled deuterium lamp (Hamamatsu Photonics, L1835) with an MgF_2 window. The monochromator (McPherson Inc., Model 234/302), based on the aberration corrected Seya-Namioka design,[64] allows for a simple rotation of the diffraction grating (Al overcoated MgF_2 with 1200 g/mm) to continuously vary the wavelength. A stepper drive system (McPherson Inc., Model 789A) was used to control the wavelength output. A National Institute of Standards and Technology (NIST) calibrated silicon photodiode detector (McPherson Inc., AXUV100G) connected with a picoammeter (Keithley Instruments, Model 6485) was used to detect the intensity of the transmitted or reflected light beams. An incident angle θ of 33° (from normal) was used in this research. The measured reflectance (R_{meas}) was calibrated using a single-side polished sapphire wafer (0001). The calibrated reflectance (R_{cal}) is given by $R_{cal} = CF \times R_{meas}$. Here, $CF = R_{ref}/R_{meas_sap}$ is the correction factor determined by taking the ratio of the measured reflectance of sapphire wafer (R_{meas_sap}) and the reference spectrum (R_{ref}) calculated using the optical constants of sapphire from literature.[27]

Surface morphology was characterized *ex situ* using an atomic force microscope (Asylum Research, MFP-3D) in alternating contact mode. Scans were taken over a $5 \times 5\,\mu m^2$ area with a scan rate of 0.5 Hz and 1024 points and lines. The cantilever used was n-type Si (AppNano, ACT-200) with a tip radius less than 10 nm. The root mean square (rms) roughness, R_q, is defined by $R_q = \sqrt{1/n \sum_{i=1}^{n} y_i^2}$, where n is the total number of points and y_i is the height of the ith point, relative to the mean line of the roughness profile.

Ex situ SE was used to deduce the optical constants (i.e., refractive index, n, and extinction coefficient, k) and the layer thicknesses. The ratio of the complex reflectance ρ of the mutually perpendicular components of the light beam (s- and p-waves) can be measured by the SE and is defined as $\rho = R_p/R_s = \tan \Psi e^{i\Delta}$, where Ψ and Δ are related to the change in amplitude and phase shift, respectively.[65] The ellipsometer (J. A. Woollam, M-2000DI) allows for use of wavelengths ranging from 193.7 to 1689.4 nm with incident angles spanning 45°–85°. Multiple incident angles, around the substrate Brewster angle, are used for more accurate measurements. An ellipsometry software package (J. A. Woollam, COMPLETEEASE v6.51) was used to analyze Ψ and Δ for the determination of thickness and optical constants. Cauchy and B-Spline dispersion models are applied for transparent and absorbing films, respectively. The root mean square error (RMSE) was used to quantify the "goodness of fit" where an RMSE of 1 indicates an ideal fit.[66]

IV. RESULTS

A. UV reflective coating

1. Surface morphology

The surface morphology of the reflective Al_2O_3/AlF_3/sapphire coating was studied by AFM. The initial sapphire surface had an rms roughness of 0.70 nm and showed polishing marks. After the deposited AlF_3 layer, the rms roughness decreased to 0.49 nm but showed specks, thought to be dust from *ex situ* transfer, and pinholes from growth. The pinholes shown in Fig. 5(b) not observed for thinner films are attributed to chamber contamination from the growth of a thick film. The largest pinhole, marked by a square, has an average depth of 3.10 nm and an rms roughness of 2.37 nm. After the final TALD Al_2O_3 layer, the surface showed a slight increase in roughness to 0.68 nm, with additional particles on the surface. The results indicate that the deposition did not roughen the surface.

2. Optical performance

The reflective coating was then characterized by UV spectroscopy and SE. The reflectance curves (Fig. 6) were measured *in situ* with the UV spectrometer (120–300 nm) and *ex situ* with the SE (193–400 nm) using incident angles θ of 33° and 45°, respectively. As the UV spectrometer was fixed, the ellipsometry software was used to convert from 45° to 33°. Since the sapphire substrate is single-side polished, the diffuse reflectance from the backside would not be detected by the detector. The discrepancy in

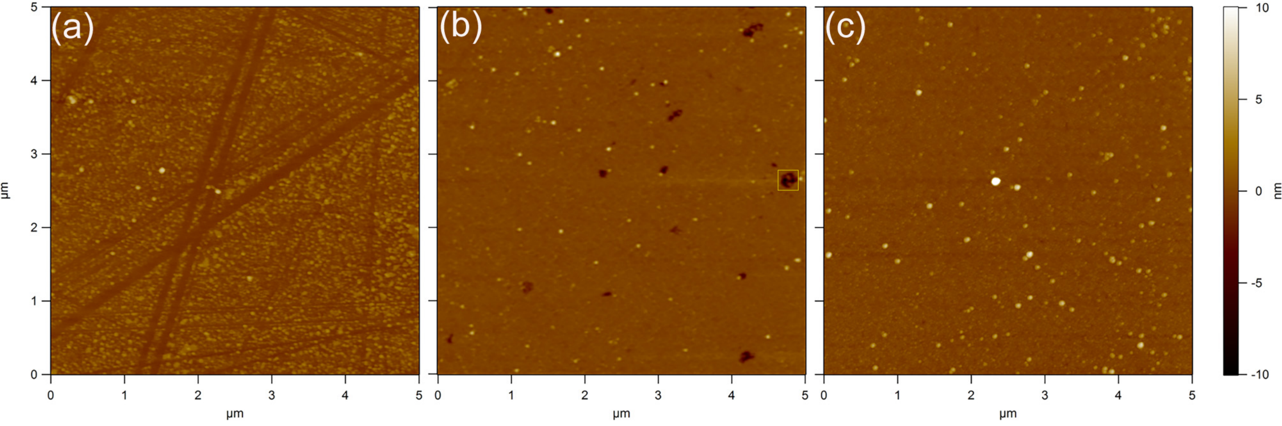

FIG. 5. AFM comparison of the middle UV coating at various stages of fabrication. (a) As received sapphire wafer showing polishing marks, $R_q = 0.70$ nm, (b) 42.8 nm of PEALD AlF_3, $R_q = 0.49$ nm, and (c) the completed coating with 32.8 nm Al_2O_3 deposited on top, $R_q = 0.68$ nm.

Published under an exclusive license by the AVS

reflectance magnitude, between the two systems, could be due to system noise, sensitivity, or atmospheric absorption (mainly O_2 at the lower wavelengths)[67] during *ex situ* SE. Measurements from the UV spectrometer showed the central wavelength, λ_{cen}, at 196 nm, which is shorter than the 212 nm target from the $m = 1$ curve ($\theta = 0°$) in Fig. 4, but agrees well with the updated design at the incident angle used in the experiment ($\theta = 33°$). Figure 6 shows that there is a significant deviation between the experiment and design in the middle UV (200–300 nm) range.

A two-term Cauchy dispersion model, with $C = 0$ in Eq. (3), was applied to characterize the refractive index of PEALD AlF_3 layer prior to the deposition of ALD Al_2O_3. An unexpected large discrepancy between the Cauchy model and the SE data, at UV wavelengths, was observed in Fig. 7, and the fitted Cauchy parameters are listed in Table II. As for the TALD grown AlF_3, the two-term Cauchy model worked well, see Fig. 4 in Hennessy *et al.*,[31] and the measured extinction coefficient, k, at $\lambda = 200$ nm is below 2.5×10^{-4}.[31,42,68] The failure of the Cauchy model to describe PEALD AlF_3 suggests the presence of impurities or defects, which are not present to the same extent in thermal ALD AlF_3.

To account for the absorption in the PEALD AlF_3 layer, a B-Spline model[69] was used to further characterize the refractive index. The measured refractive index of $n = 1.44$ at 589 nm is higher than $n = 1.36$ reported by several other groups for ALD AlF_3,[31,42,68,70] and $n = 1.38$ for bulk AlF_3.[71] The resulting extinction coefficient k was identified to start increasing at 400 nm and reach a maximum at ∼221 nm (Fig. 8).

As for the TALD Al_2O_3 layer, the determined Cauchy parameters are A = 1.628, B = 0.005 05, and C = 0.000 143 39.

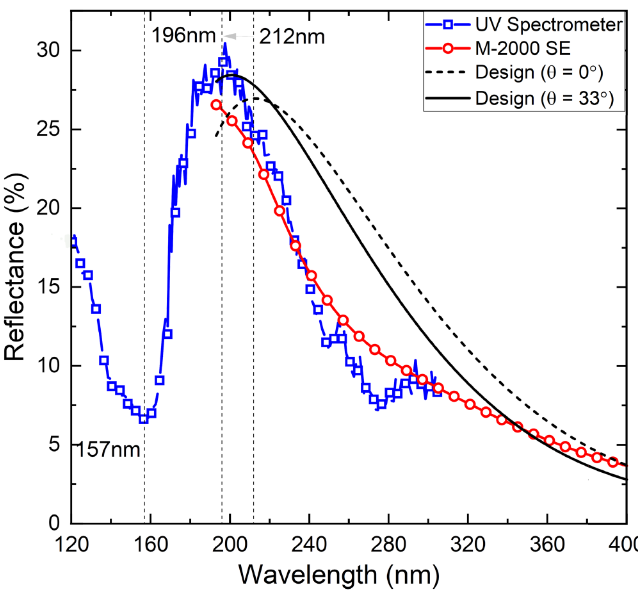

FIG. 6. Unpolarized reflectance measured using the M-2000 SE and UV spectrometer.

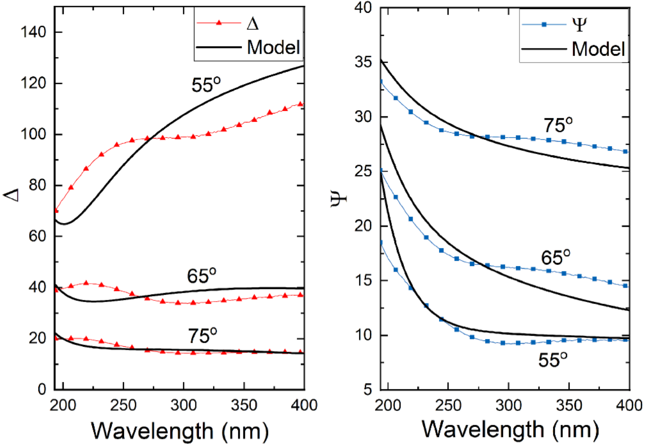

FIG. 7. Ellipsometric parameters, Ψ and Δ, for PEALD AlF_3 on sapphire.

The measured refractive index $n = 1.64$ at 630 nm agrees with $n = 1.65–1.66$ for TALD Al_2O_3.[72,73] The determined thicknesses of each layer are 42.8 nm for PEALD AlF_3 and 32.8 nm for TALD Al_2O_3. The corresponding growth rate for the PEALD AlF_3 film was 1.3 Å/cycle. The determined thickness is slightly different from the target value [Fig. 3(b)], which is most likely due to the deposition with inaccurate growth rate determined for PEALD AlF_3. Regardless of the unexpected absorption in the AlF_3 layer, the UV reflectance (Fig. 6) shows a peak reflectance of 25%–30% at 196 nm, with a bandwidth of about 50 nm.

B. Origin of absorption in PEALD AlF_3

1. X-ray photoelectron spectroscopy

The optical measurements on the UV filter suggested defects in the PEALD AlF_3 that exist to a greater extent than thermal ALD AlF_3. Consequently, a careful comparison of the chemical bonding of PEALD and TALD AlF_3 films was initiated using XPS. As noted previously, PEALD and TALD AlF_3 films were on Si substrates passivated with Al_2O_3. 40 cycles of ALD was performed for each AlF_3 film. The Al 2p scans for the layers are compared in Fig. 9. The different peaks are associated with the chemical shifts of Al atoms bonded to O, F, and Al. The peak parameters from the scans are listed in Table III.

XPS spectra of the Al 2p region are shown in Fig. 9 for both ALD AlF_3 films. The PEALD AlF_3 Al 2p scan showed the presence of a third, low binding energy peak at 73.1 eV, interpreted as an

TABLE II. Cauchy parameters characterized for ALD AlF_3.

Reference	Method	A	B	RMSE
This work	PEALD	1.418 ± 0.005	0.0187 ± 0.0019	29.358
Hennessy *et al.* (Ref. 31)	TALD	1.352 ± 0.005	0.0019 ± 0.0002	N/A

Published under an exclusive license by the AVS

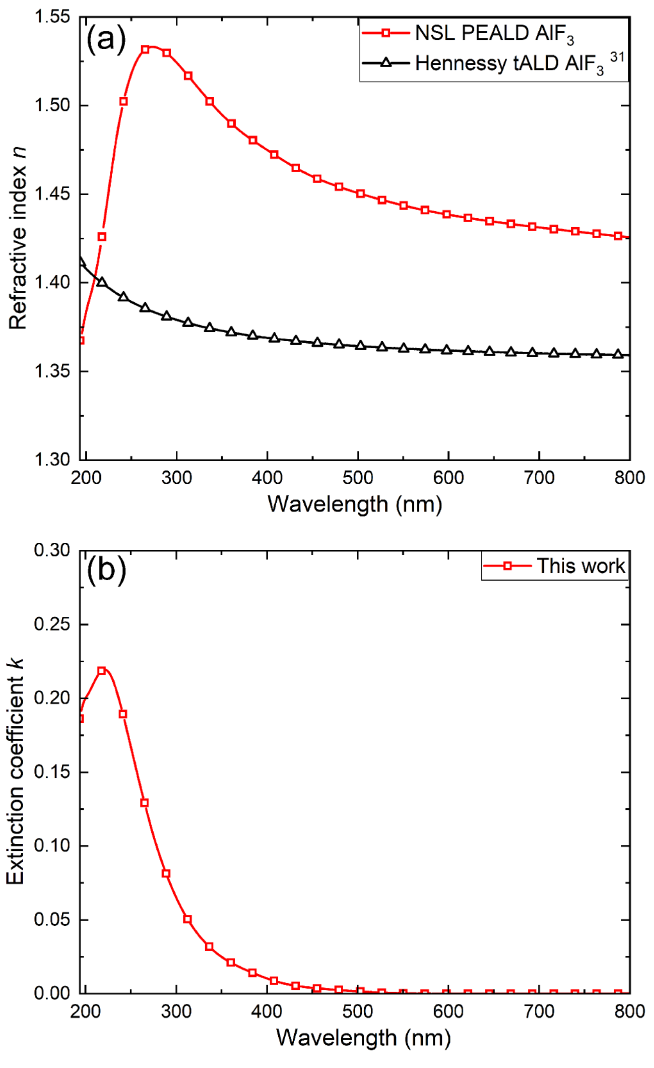

FIG. 8. Optical constants of PEALD AlF_3, determined by the B-Spline model. (a) Refractive index *n* and (b) extinction coefficient *k*.

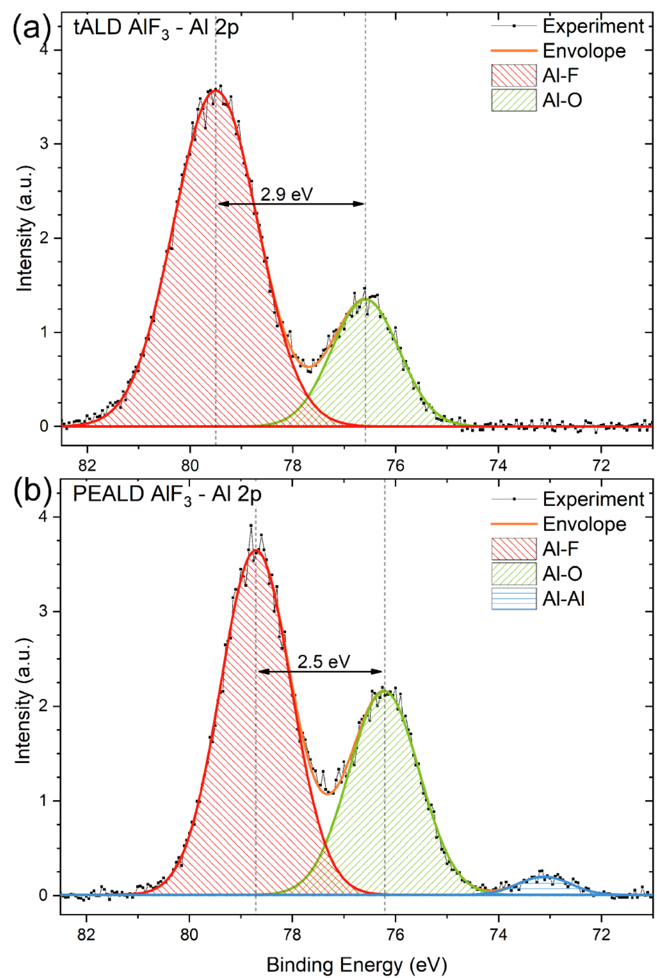

FIG. 9. XPS Al 2p spectra of ALD AlF_3 films on 33 nm TALD Al_2O_3. The peaks associated with AlF_3, Al_2O_3, and Al clusters (blue) are shown. (b) PEALD AlF_3 shows the presence of an Al-Al bonding that is absent for (a) TALD AlF_3.

Al-Al chemical state[63] [Fig. 9(b)]. This Al-Al chemical state was not observed for the TALD film and is thought to occur during the H_2-plasma step. The Al-Al chemical state could indicate the presence of Al-rich clusters in the PEALD AlF_3 layer at 4.8 ± 0.95 at. %. Additionally, a change in peak profile was observed for the PEALD AlF_3 Al-F chemical state (Table III). The change in peak position and FWHM is likely related to the presence of Al-rich clusters.

The presence of carbon and oxygen in the AlF_3 films was also analyzed by XPS. Some carbon (∼3 at. %) was observed in the TALD passivating Al_2O_3 layer prior to growth of the AlF_3. Additional carbon was not detected after TALD or PEALD AlF_3 film growth. Additionally, both TALD and PEALD AlF_3 films showed the presence of a second peak in the F 1s and O 1s spectra thought to indicate the presence of an AlO_xF_y layer. In a study of

TABLE III. Comparison of the Al 2p XPS peak parameters for before and after deposition of TALD and PEALD AlF_3 film. Errors are calculated from peak fitting and instrument resolution. Unless listed, errors were less than 0.1 eV.

		Chemical state (Al 2p)	Peak energy (eV)	Peak width FWHM (eV)	Peak area (eV cts/s)
TALD	Before	Al-O	76.0	1.5	10.6
	After	Al-O	76.6 ± 0.1	1.5	2.2
		Al-F	79.5	1.9	7.3
PEALD	Before	Al-O	75.9	1.5	11.3
	After	Al-O	76.2	1.6	3.7
		Al-F	78.7	1.6	6.3
		Al-Al	73.1 ± 0.1	1.2 ± 0.2	0.3

Published under an exclusive license by the AVS

water adsorption on AlF_3 surfaces, corresponding additional peaks were observed.[31,74] We speculate that the AlO_xF_y layer could be at the Al_2O_3-AlF_3 interface or on the AlF_3 surface. Comparison of the two F 1s peak fitted areas showed the AlO_xF_y layer consisted of $4.5 \pm 0.90\%$ and $5.3 \pm 1.0\%$ of the photoelectron signal for the TALD and PEALD and AlF_3, respectively. From the SE measurements, the PEALD AlF_3 film thickness was estimated to be 5.2 nm with a growth rate of 1.3 Å/cycle. Previous data indicated that the TALD AlF_3 films had a growth rate of 1.5 Å/cycle for a thickness of 5.8 nm. The TALD AlF_3 growth rate is within 7.1% of AlF_3 grown using the same precursors and temperature.[42] Based on the AlF_3 layers, the AlO_xF_y layer thicknesses would be 2.6 ± 0.5 and 1.8 ± 0.4 Å for the TALD and PEALD AlF_3 films, respectively. While the integrated peak areas of the Al 2p and F 1s core levels are similar for both ALD AlF_3 films, a careful analysis would be needed to accurately determine the Al:F ratios due to the significant differences in the Al-F chemical state FWHMs.

The XPS results indicated that neither the plasma enhanced nor thermal ALD AlF_3 films showed a detectable increase in carbon after ALD. Both films indicated the presence of interfacial AlO_xF_y thought to have a subnanometer thickness. The growth per cycle of TALD was comparable to reported values while the PEALD growth rate was ∼7% lower. The PEALD AlF_3 film showed a third peak, in the Al 2p region, interpreted as Al–Al bonding. The Al–Al bonds are thought to correspond to Al-rich clusters. The relative concentration of the Al-rich clusters was calculated, based on the ratio of Al-F to Al-Al peak areas. The results indicated the Al-rich clusters composed 4.8 ± 0.95 at. %, of the AlF_3 layer. It is likely that this component is responsible for the observed absorption in the middle UV.

2. Optical characterization

This section considers the optical properties of a 5.2 nm PEALD and a 5.8 nm TALD AlF_3 film deposited on 33 nm TALD Al_2O_3/Si, which were characterized by SE. Using a B-spline model, the maximum extinction coefficient, k_m, of the TALD AlF_3 film was determined to be 0.06, at wavelengths between 200 and 400 nm. For PEALD AlF_3 film, k_m is 0.30 over the same range. Combined with the XPS analysis (Fig. 9), it is evident that the Al-rich clusters component, observed in the PEALD AlF_3 film, contributes to the observed absorption.

SE was further used to study the Al clusters concentration within the PEALD AlF_3 films on sapphire by employing the effective medium approximations (EMA) method.[75] In EMA theory, an effective dielectric function (ε_{EMA}) is used to describe a composite with two constituents, where $\varepsilon_{EMA} = f_a\varepsilon_a + f_b\varepsilon_b$ with the constraint $f_a + f_b = 1$. Here (f_a, f_b) and (ε_a, ε_b) are the volume fraction and dielectric functions of each constituent, respectively. The measured optical constants of PEALD AlF_3 (Fig. 8) were fit using the Bruggeman EMA method[69,75] [Fig. 10(a)] to determine the volume fraction of the Al-rich clusters. The optical constants used for AlF_3 and Al are from the results for thermal ALD AlF_3 (193.7–400 nm)[31] and evaporated Al metal (138–400 nm),[76] respectively [Fig. 10(b)]. For AlF_3, the refractive index at wavelengths 138–193.7 nm is obtained by extending the Cauchy model for thermal ALD AlF_3, by assuming the absorption is negligible in this wavelength range. This assumption is reasonable as the extinction coefficient for thermally evaporated AlF_3 is reported to be below 8×10^{-3} in the region of interest.[77] From the Bruggeman EMA analysis, the volume fraction of the Al-rich clusters was found to be 2.4 ± 0.02 vol. %, which can be roughly converted to an atomic concentration of 7.8 at. %. The density used in this conversion is 2.9 g/cm^3 for TALD AlF_3 films[42] and 2.61 g/cm^3 for evaporated Al films.[78] Consequently, including 2.4 vol. % Al clusters in the PEALD AlF_3 layers, the RMSE of the fitting in Fig. 7 has been reduced from 29.36 to 5.01. To simulate the reflectivity at wavelengths 138–193.7 nm, the optical constants of PEALD AlF_3 were

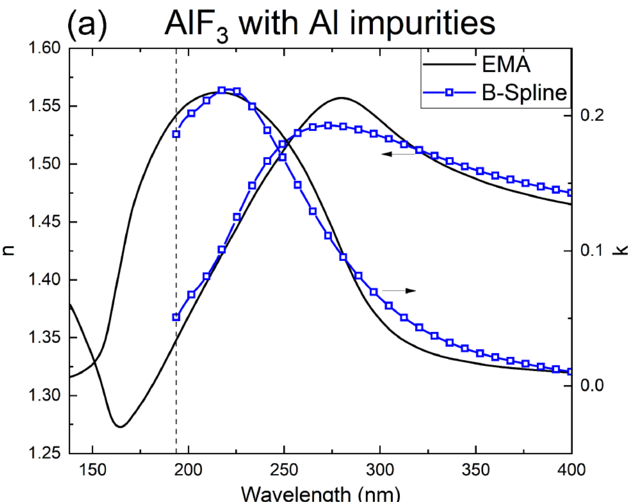

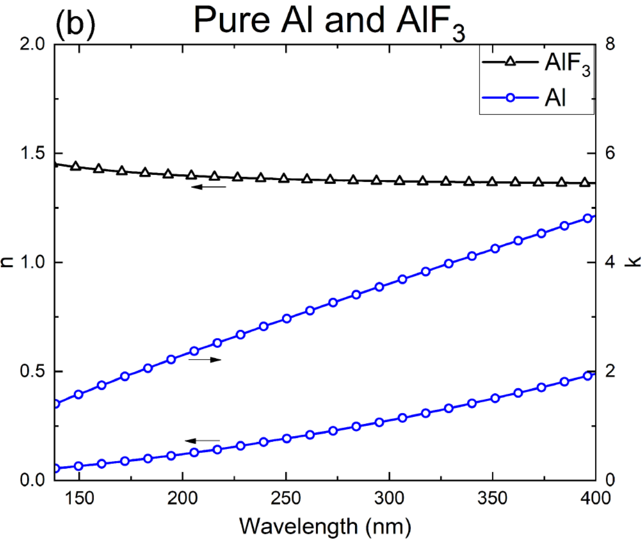

FIG. 10. Bruggeman EMA analysis of PEALD AlF_3 where the B-Spline curve corresponds to the experimental SE data of the layer. (a) Effective optical constants obtained with 2.4 vol. % Al clusters in the AlF_3 films, at wavelengths between 138 and 400 nm. (b) Optical constants of pure AlF_3 (Ref. 31) and Al (Ref. 76) in the same wavelength range.

Published under an exclusive license by the AVS

generated by mixing the optical constants of pure Al and AlF_3 using the Bruggeman EMA method. The simulated reflectivity in the wavelength range 138–400 nm is shown in Fig. 11(a).

V. DISCUSSION

A. XPS results for AlF_3

The most significant observation is the presence of Al-rich clusters in the PEALD layer at a level of 4.8 ± 0.95 at. %, which is close to the 7.80 at. % determined by SE analysis. Additionally, the AlF_3 showed the presence of AlO_xF_y likely with subnanometer thickness. Thicker films (>12 nm) would be required to determine the location of the interfacial oxyfluoride by fully attenuating the substrate photoelectron signal. Additional carbon was not detected after PEALD AlF_3 growth, which likely precludes carbon as the source of the optical absorption. The mechanism for the formation of these Al-rich clusters is not understood but is thought to originate during the H_2-plasma step.

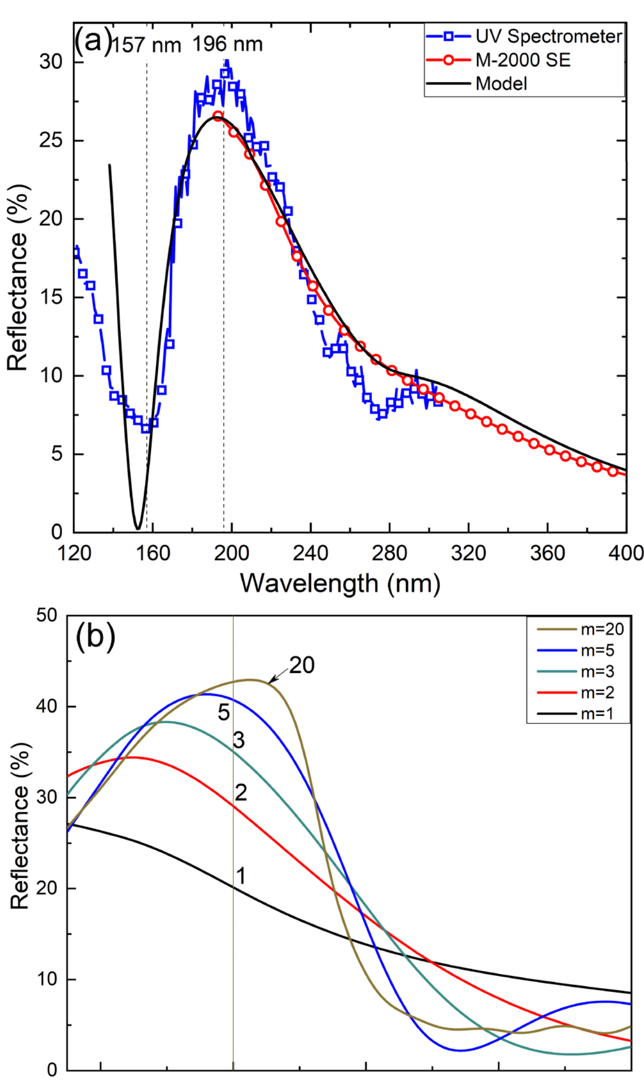

FIG. 11. Optical modeling of the reflective coating. (a) Modeling of the reflectance below 193.7 nm, with 2.4 vol. % Al clusters considered in the AlF_3 films. (b) Simulated reflectance of the reflective coating with the updated optical constants from Fig. 8.

B. Optical performance for the reflective coating

The presence of the Al-rich clusters will affect the optical properties of the layer and multilayer filter. Figure 11(a) shows the modeled reflectance curve of the UV coating in the wavelength range of 138–400 nm, using the EMA optical constants of PEALD AlF_3 in Fig. 10(a). The modeled curve showed a "dip" at around 157 nm, which agrees with the experiments. The simulation for the multilayer reflective coating updated with the optical constants from Fig. 8 is shown in Fig. 11(b). The ultimate reflectance has been degraded from 100% to 43%, and the central wavelength also varies with the number of repeating bilayers, which is different from the original design shown in Fig. 4. This implies that reducing or eliminating Al-rich clusters in the AlF_3 deposition should enable filters with greater reflectivity. Long deposition times, for the AlF_3 and Al_2O_3 layers, precluded a second round of experiments using modified ALD parameters.

VI. SUMMARY AND CONCLUSIONS

A multilayer high-reflective coating, based on AlF_3 and Al_2O_3, has been designed and fabricated. SE measurements of the reflective coating suggested the presence of an absorbing compound inside the PEALD AlF_3 layer. To determine the cause of absorption, a set of PEALD and TALD AlF_3 films was grown and characterized by XPS and SE. The results implied the existence of Al-rich clusters in the PEALD AlF_3 films. Further analysis on the differences in growth characteristics and material properties, for the TALD and PEALD AlF_3 film, is planned.[79] Optical simulations suggest that the incorporation of Al-rich clusters (~2.4 vol. %) into the AlF_3 layer would cause a reflectance deviation in the middle UV wavelength.

Further studies are needed to determine the cause of Al-cluster formation and a method to mitigate their formation in PEALD AlF_3 films. Otherwise, TALD AlF_3 would be preferred for UV optical coatings. Additionally, the ALD interface impurities could be reduced by combining the AlF_3 and Al_2O_3 depositions in the same reactor or interconnected chambers. Besides Al_2O_3 and AlF_3, other dielectric materials, including HfO_2, MgF_2, and LiF, could be applied to UV optics. Further improvement of the optical modeling could be achieved by determination of the film UV optical constants.

In summary, this work demonstrated the use of ALD to fabricate an all-dielectric high-reflectivity middle UV coating. The work supports a path forward for middle and even far UV optical filters and devices. Various issues have been identified with solutions proposed for future research of materials for UV optics.

Published under an exclusive license by the AVS

ACKNOWLEDGMENTS

This research was supported through the National Aeronautics and Space Administration under Grant No. NNH14ZDA001N-SAT. We acknowledge the use of facilities within the Eyring Materials Center at the Arizona State University. We thank Jaime Quintero from the ASU NanoFab for the growth of Al_2O_3 films, and Hongbin Yu (ASU), Tom Mooney (Materion), and Matt Beasley (Planetary Resources Inc.) for fruitful discussions. We would like to thank our colleagues Yichen Yao for assistance in the growth of Al_2O_3 films and Xingye Wang for assistance in the assembling the ALD reactor.

DATA AVAILABILITY

The data that support the findings of this study are available from the corresponding author upon reasonable request.

REFERENCES

[1] G. Christidis *et al.*, ACS Appl. Mater. Interfaces **12**, 9925 (2020).
[2] H. W. Moos *et al.*, Astrophys. J. **538**, L1 (2000).
[3] P. Ribes-Pleguezuelo, F. Keller, and M. Taccola, e-print arXiv:2006.14967 [astro-ph.IM] (2020).
[4] B. Fleming *et al.*, Appl. Opt. **56**, 9941 (2017).
[5] G. A. Gary, E. A. West, D. Rees, J. A. Mckay, M. Zukic, and P. Herman, Astron. Astrophys. **461**, 707 (2007).
[6] L. Yuan, Y. N. Zhao, C. J. Wang, H. B. He, Z. X. Fan, and J. D. Shao, Appl. Surf. Sci. **253**, 3450 (2007).
[7] S. Gunster, D. Ristau, A. Gatto, N. Kaiser, M. Trovo, and M. Danailov, Appl. Opt. **45**, 5866 (2006).
[8] M. S. Alias *et al.*, IEEE Photonics J. **10**, 1 (2018).
[9] F. Réveret *et al.*, J. Appl. Phys. **120**, 093107 (2016).
[10] T. Sertel, Y. Ozen, V. Baran, and S. Ozcelik, J. Alloys Compd. **806**, 439 (2019).
[11] H. A. Macleod, in *Thin-Film Optical Filters*, edited by E. R. Pike and R. G. W. Brown (CRC, Boca Raton, 2018), Chap. 6, pp. 183–212.
[12] M. Zukic, D. G. Torr, J. F. Spann, and M. R. Torr, Appl. Opt. **29**, 4293 (1990).
[13] M. Zukic and D. G. Torr, Appl. Opt. **31**, 1588 (1992).
[14] J. I. Larruquert, in *Optical Thin Films and Coatings*, edited by A. Piegari and F. Flory (Woodhead, Cambridge, 2018), Chap. 7, pp. 291–356.
[15] M. Beasley, F. Greer, and S. Nikzad, Proc. SPIE **8443**, 84433Q (2012).
[16] J. Sun, X. Li, W. L. Zhang, K. Yi, and J. D. Shao, Opt. Laser Technol. **56**, 65 (2014).
[17] V. S. P. Kumar, M. Kumar, N. Kumari, V. Karar, and A. L. Sharma, Mater. Res. Express **6**, 066410 (2019).
[18] S. F. Pellicori, C. L. Martinez, P. Hausgen, and D. Wilt, Appl. Opt. **53**, A339 (2014).
[19] E. S. Field, J. C. Bellum, and D. E. Kletecka, Proc. SPIE **8885**, 88851X (2013).
[20] P. Torchio, A. Gatto, M. Alvisi, G. Albrand, N. Kaiser, and C. Amra, Appl. Opt. **41**, 3256 (2002).
[21] X. D. Wang, B. Chen, and L. Yao, Appl. Spectrosc. **72**, 943 (2018).
[22] M. C. Liu, C. C. Lee, B. H. Liao, M. Kaneko, K. Nakahira, and Y. Takano, Appl. Opt. **47**, C214 (2008).
[23] T. Nakashima, K. Takeda, H. Shinzato, M. Iwaya, S. Kamiyama, T. Takeuchi, I. Akasaki, and H. Amano, Jpn. J. Appl. Phys. **52**, 08JG07 (2013).
[24] M. Fernandez-Perea, M. Vidal-Dasilva, J. I. Larruquert, J. A. Mendez, and J. A. Aznarez, Astrophys. Space Sci. **320**, 243 (2009).
[25] M. Jerman, Z. Qiao, and D. Mergel, Appl. Opt. **44**, 3006 (2005).
[26] M. F. Al-Kuhaili, Opt. Mater. **27**, 383 (2004).
[27] M. J. Dodge, in *Handbook of Laser Science and Technology*, edited by M. J. Weber (CRC, Boca Raton, FL, 1986), Vol. IV, p. 30.
[28] G. Ghosh, Opt. Commun. **163**, 95 (1999).
[29] L. V. Rodriguez-de Marcos, J. I. Larruquert, J. A. Mendez, and J. A. Aznarez, Opt. Mater. Express **7**, 989 (2017).
[30] H. H. Li, J. Phys. Chem. Ref. Data **9**, 161 (1980).
[31] J. Hennessy, A. Jewell, K. Balasubramanian, and S. Nikzad, J. Vac. Sci. Technol. A **34**, 01A120 (2016).
[32] P. O. Oviroh, R. Akbarzadeh, D. Pan, R. A. M. Coetzee, and T.-C. Jen, Sci. Technol. Adv. Mater. **20**, 465 (2019).
[33] S. M. George, Chem. Rev. **110**, 111 (2010).
[34] J. Robertson, Eur. Phys. J. Appl. Phys. **28**, 265 (2004).
[35] R. W. Johnson, A. Hultqvist, and S. F. Bent, Mater. Today **17**, 236 (2014).
[36] P. French, G. Krijnen, and F. Roozeboom, Microsyst. Nanoeng. **2**, 16048 (2016).
[37] S. Zhuiykov, T. Kawaguchi, Z. Hai, M. Karbalaei Akbari, and P. M. Heynderickx, Appl. Surf. Sci. **392**, 231 (2017).
[38] B. Groven *et al.*, Chem. Mater. **29**, 2927 (2017).
[39] H. B. Profijt, S. E. Potts, M. C. M. van de Sanden, and W. M. M. Kessels, J. Vac. Sci. Technol. A **29**, 050801 (2011).
[40] C. Q. Hu, J. Z. Cai, Y. K. Li, C. B. Bi, Z. Q. Gu, J. Q. Zhu, J. F. Zang, and W. T. Zheng, J. Mater. Chem. C **8**, 3248 (2020).
[41] P. A. Premkumar, A. Delabie, L. N. J. Rodriguez, A. Moussa, and C. Adelmann, J. Vac. Sci. Technol. A **31**, 061501 (2013).
[42] Y. Lee, J. W. DuMont, A. S. Cavanagh, and S. M. George, J. Phys. Chem. C **119**, 14185 (2015).
[43] M. Zukic, D. G. Torr, J. M. Kim, J. F. Spann, and M. R. Torr, Opt. Eng. **32**, 3069 (1993).
[44] S. K. Tripathy, Opt. Mater. **46**, 240 (2015).
[45] D. König, R. Scholz, D. R. T. Zahn, and G. Ebest, J. Appl. Phys. **97**, 093707 (2005).
[46] A. Belosludtsev, K. Juškevičius, L. Ceizaris, R. Samuilovas, S. Stanionytė, V. Jasulaitienė, and S. Kičas, Appl. Surf. Sci. **427**, 312 (2018).
[47] R. K. Choudhary, P. Mishra, A. Biswas, and A. C. Bidaye, ISRN Mater. Sci. **2013**, 1 (2013).
[48] I. Bhaumik, R. Bhatt, S. Ganesamoorthy, A. Saxena, A. K. Karnal, P. K. Gupta, A. K. Sinha, and S. K. Deb, Appl. Opt. **50**, 6006 (2011).
[49] S.-L. Ku and C.-C. Lee, Opt. Mater. **32**, 956 (2010).
[50] K.-N. Chen, C.-M. Hsu, J. Liu, Y.-C. Liou, and C.-F. Yang, Micromachines **7**, 151 (2016).
[51] T. Siefke *et al.*, Adv. Opt. Mater. **4**, 1780 (2016).
[52] F. Z. Tepehan, F. E. Ghodsi, N. Ozer, and G. G. Tepehan, Sol. Energy Mater. Sol. Cells **46**, 311 (1997).
[53] L. V. Rodríguez-de Marcos, J. I. Larruquert, J. A. Méndez, and J. A. Aznárez, Opt. Mater. Express **6**, 3622 (2016).
[54] J.-K. Yang, W. S. Kim, and H.-H. Park, Thin Solid Films **494**, 311 (2006).
[55] M. L. Huang, Y. C. Chang, C. H. Chang, T. D. Lin, J. Kwo, T. B. Wu, and M. Hong, Appl. Phys. Lett. **89**, 012903 (2006).
[56] E. R. Zakirov, V. G. Kesler, G. Y. Sidorov, I. P. Prosvirin, A. K. Gutakovsky, and V. I. Vdovin, Semicond. Sci. Technol. **34**, 065007 (2019).
[57] J. Hennessy and S. Nikzad, Inorganics **6**, 46 (2018).
[58] C. C. Katsidis and D. I. Siapkas, Appl. Opt. **41**, 3978 (2002).
[59] B. Harbecke, Appl. Phys. B **39**, 165 (1986).
[60] P. Scowen, D. C. Messina, Z. Huang, B. Eller, R. J. Nemanich, H. Yu, T. Mooney, and M. Beasley, see http://www.astrostrategictech.us/pdf/projectfiles/Reports/14-SAT14-0023_AR_Scowen_Paul_2019_06.pdf (accessed February 24, 2021).
[61] G. A. Olah, J. T. Welch, Y. D. Vankar, M. Nojima, I. Kerekes, and J. A. Olah, J. Org. Chem. **44**, 3872 (1979).
[62] S. Tougaard, Surf. Interface Anal. **25**, 137 (1997).
[63] J. F. Moulder, W. F. Stickle, P. E. Sobol, and K. D. Bomben, *Handbook of X-ray Photoelectron Spectroscopy* (Perkin-Elmer Corporation, Eden Prairie, MN, 1979), Chap. 1, p. 25.
[64] T. Namioka, J. Opt. Soc. Am. **49**, 951 (1959).
[65] H. Fujiwara, in *Spectroscopic Ellipsometry for Photovoltaics*, edited by H. Fujiwara and R. W. Collins (Springer International Publishing AG, Cham, 2018), Chap. 1.1.1., Vol. 1, pp. 2–5.
[66] J.A. Woollam Co., *CompleteEASE Software Manual* (J.A. Woollam Co., Lincoln, NE, 2014), Chap. 3.1, pp. 48–51.

Published under an exclusive license by the AVS

[67]D. G. Andrews, *An Introduction to Atmospheric Physics* (Cambridge University, New York, 2010), Chap. 3.5, p. 71.
[68]M. F. J. Vos, H. C. M. Knoops, R. A. Synowicki, W. M. M. Kessels, and A. J. M. Mackus, Appl. Phys. Lett. **111**, 113105 (2017).
[69]J.A. Woollam Co., *CompleteEASE Software Manual* (J.A. Woollam Co., Lincoln, NE, 2014), Chap. 4.3, pp. 118–125.
[70]M. Mäntymäki, M. J. Heikkilä, E. Puukilainen, K. Mizohata, B. Marchand, J. Räisänen, M. Ritala, and M. Leskelä, Chem. Mater. **27**, 604 (2015).
[71]E. Staritzky and L. B. Asprey, Anal. Chem. **29**, 984 (1957).
[72]C. Barbos, D. Blanc-Pelissier, A. Fave, C. Botella, P. Regreny, G. Grenet, E. Blanquet, A. Crisci, and M. Lemiti, Thin Solid Films **617**, 108 (2016).
[73]M. Broas, O. Kanninen, V. Vuorinen, M. Tilli, and M. Paulasto-Kröckel, ACS Omega **2**, 3390 (2017).
[74]A. Makarowicz, C. L. Bailey, N. Weiher, E. Kemnitz, S. L. M. Schroeder, S. Mukhopadhyay, A. Wander, B. G. Searle, and N. M. Harrison, Phys. Chem. Chem. Phys. **11**, 5664 (2009).
[75]J. N. Hilfiker, J. Sun, and N. Hong, in *Spectroscopic Ellipsometry for Photovoltaics*, edited by H. Fujiwara and R. W. Collins (Springer International Publishing AG, Cham, 2018), Chap. 3, Vol. 1, pp. 59–88.
[76]D. Y. Smith, E. Shiles, and M. Inokuti, in *Handbook of Optical Constants of Solids*, edited by E. D. Palik (Elsevier, New York, 1997), Vol. 1, p. 369.
[77]S. Günstera *et al.*, Proc. SPIE **5250**, 146 (2004).
[78]T. E. Hartman, J. Vac. Sci. Technol. **2**, 239 (1965).
[79]D. C. Messina, B. S. Eller, P. Scowen, and R. J. Nemanich, "Comparison of AlF_3 thin films grown by thermal and plasma enhanced atomic layer deposition" (unpublished).

Published under an exclusive license by the AVS